# Automatic blush detection in 'concealed information' test using visual stimuli

Shigang Yue*

Lincoln School of Computer Science,
University of Lincoln,
Brayford Pool Campus,
Lincoln, LN6 7TS, UK
Fax: +44-1522-88-6974
E-mail: syue@lincoln.ac.uk
*Corresponding author

Karl Harmer

School of Engineering and Digital Arts,
University of Kent,
Canterbury, Kent, CT2 7NZ, UK
E-mail: karlharmer@googlemail.com

Kun Guo and Karen Adams

School of Psychology,
University of Lincoln,
Lincoln, LN6 7TS, UK
E-mail: kguo@lincoln.ac.uk
E-mail: karenmichelle.adams@gmail.com

Andrew Hunter

School of Computer Science,
University of Lincoln,
Lincoln, LN6 7TS, UK
E-mail: ahunter@lincoln.ac.uk

**Abstract:** Blushing has been identified as an indicator of deception, shame, anxiety and embarrassment. Although normally associated with the skin coloration of the face, a blush response also affects skin surface temperature. In this paper, an approach to detect a blush response automatically is presented using the Argus P7225 thermal camera from e2v. The algorithm was tested on a sample population of 51 subjects, while using visual stimuli to elicit a response, and achieved recognition rates of ~77% TPR and ~60% TNR, indicating a thermal image sensor is the prospective device to pick up subtle temperature change synchronised with stimuli.

**Keywords:** blush detection; thermal image; psychophysiology; deception; visual cues; temperature change.

**Reference** to this paper should be made as follows: Yue, S., Harmer, K., Guo, K., Adams, K. and Hunter, A. (2014) 'Automatic blush detection in 'concealed information' test using visual stimuli', *Int. J. Data Mining, Modelling and Management*, Vol. 6, No. 2, pp.187–201.

**Biographical notes:** Shigang Yue is a Reader in the School of Computer Science, University of Lincoln, UK. He received his PhD from Beijing University of Technology (BJUT) in 1996 and worked in BJUT as Lecturer and Associate Professor till 2000. Before joining the University of Lincoln in 2007, he held research positions in University of Cambridge, University of Newcastle and University College London, respectively. His research interests are mainly within the field of artificial intelligence, computer vision, robotics, brains, and neuroscience. He has published more than 50 journal and conference papers in the above fields.

Karl Harmer received his MEng in Electronic and Computer Systems Engineering from Loughborough University, UK, in 2003 and his PhD in Electronic Engineering from the University of Kent, UK, in 2010. He is currently a Post-Doctoral Researcher at the University of Kent with research interests in biometrics, image and signal processing, pattern recognition, and data security.

Kun Gu is a Reader in Cognitive Neuroscience in School of Psychology, University of Lincoln, UK. He earned his BSc in Human Physiology from Nanjing University and PhD in Visual Neuroscience from Chinese Academy of Sciences, and undertook postdoctoral training in cognitive neuroscience at Oxford University and Newcastle University. With combined methods of neurophysiology, eye-tracking, psychophysics assessment and computational modelling, his current research is focused on two topics: exploitation of environmental regularities in visual process, and processing of facial and body cues in social communication and human-animal interactions.

Karen Adams obtained her BSc and PhD in Psychology from the University of Lincoln. Her PhD (awarded in 2009) looked at the techniques and methods used in assessing human visual acuity, principally those that are not reliant on a verbal response. She also considered how new vision tests might best be developed. She is particularly interested in gaze perception and how accurately we can determine the gaze direction of another person. She has worked on projects examining the visual search skills of expert fingerprint officers and measuring psychophysiological responses elicited by visual stimuli in concealed information tests.

Andrew Hunter is Pro-Vice Chancellor and Head of the College of Science at the University of Lincoln, having formerly held academic positions at the Universities of Durham and Sunderland and worked in industry as a Software Engineer. His research interests are in computer vision, sensor interpretation, neurally-inspired hardware pattern recognition and retinal image analysis. He has published over 100 academic papers, including more than 30 in international peer-reviewed journals, and is the author of several software packages, including the public-domain genetic algorithm simulator Sugal, and the neural network simulation package Trajan.

This paper is a revised and expanded version of a paper entitled 'Automatic blush detection in 'concealed information' test using visual stimuli' presented at the International Conference on Soft Computing and Pattern Recognition (SoCPaR 2010), Cergy-Pontoise, Paris, France, 7–10 December 2010.

## 1 Introduction

The ability to detect deception is a highly desirable quality. The act of deception is prevalent and the consequences of concealing the truth cover a broad range of severity. At one extreme, a harmless white lie will have minimal repercussions. However, at the other extreme, human lives could be in danger. Therefore, research continues unabated in the pursuit of accurate identification of deceit.

When a person is attempting to conceal the truth, the underlying emotional response can manifest in measurable physiological characteristics (Pavlidis et al., 2002). Blushing has been identified as one of these characteristics (Pollina et al., 2006) as has, among others, heart rate (Pavlidis et al., 2002; Vershuere et al., 2004), respiration rate (Gamer et al., 2006), perspiration (Gronau et al., 2005) and blink rate (Fukuda, 2001). Any combination of which can indicate deception.

On the face of it, blushing seems a trivial task. Essentially, it is simply a matter of analysing the temperature or coloration of the skin with respect to the time a stressor (in this case, visual stimulus) is presented to the subject. In fact, there is much research regarding the blush response to a stressor in the fields of psychology and psychophysiology (Mulkens et al., 1997, 1999; DeJong et al., 2002; Shearn et al., 1990; Drummond and Lim, 2000). These approaches either require contact with the subject using transducers (commonly plethysmographic transducers) (Mulkens et al., 1997, 1999; DeJong et al., 2002; Shearn et al., 1990; Drummond and Lim, 2000) and/or thermisters (Mulkens et al., 1997; Shearn et al., 1990; Drummond and Lim, 2000). Even when thermal images are used, the region of interest (ROI) is often manually segmented (Pollina et al., 2006; Mulkenset al., 1999).

Unfortunately, at present, there does not appear to be an abundance of fully automated segmentation methods available. This might suggest that researchers, at this time, are content with manual segmentation (i.e., where a practical implementation is not necessary). However, as the interest in the field and detection accuracy increases, fully automated systems will follow which will require a general-purpose segmentation algorithm.

In order to develop a fully-automated segmentation algorithm, the ROI needs to be identified. In Kalra and Magnenat-Thalmann (1994), they state that the action of blushing is revealed more from the cheeks, ears and forehead than from any other body part. In Zhu et al. (2007, 2008), the supraorbital vessels of the forehead are extracted by employing the Hough transform in the forehead region to extract the approximate location of the vessels. An active contour method is then applied to determine the central lines of the vessels before extracting the boundaries. Whereas in Shastri et al. (2008) and Tsiamyrtzis et al. (2005), the periorbital region is extracted using the eye location as a point of reference to define the initial periorbital region that is then tracked throughout the footage. However, the problem with using the forehead, ears or periorbital regions is occlusion. The forehead and ears can easily be covered by hair and the periorbital region is often occluded by spectacles.

In a typical real-life scenario, subjects will have varying hairstyles, headwear and spectacles. The most consistently visible ROI is the region around the maxilla. The maxilla region can also be visible in people with full beards. In Pollina et al. (2006), this region is used as the ROI. However, the exact method of segmentation is not described. Therefore, in this paper, an algorithm is outlined which can be employed to extract a

consistent ROI in thermal images. The next section of this paper presents the proposed ROI segmentation algorithm, subsequently followed by the proposed blush detection criteria. This is followed by the experimental results with respect to an application employing visual stimuli to elicit a blush response. Finally, conclusions are drawn with remarks about possible improvements.

## 2 Proposed segmentation algorithm

The detection of blush is essentially a segmentation problem. The behaviour of temperature during a blush response is well documented (Mulkens et al., 1997, 1999; DeJong et al., 2002; Shearn et al., 1990; Drummond and Lim, 2000) and therefore, given a consistent ROI, the temperature trend of that ROI can be analysed. However, ensuring that the same relative region is segmented in all frames is not as straightforward, especially if free head movement is permitted. In Figure 1, a basic framework is presented for segmenting the ROI.

**Figure 1** ROI segmentation framework

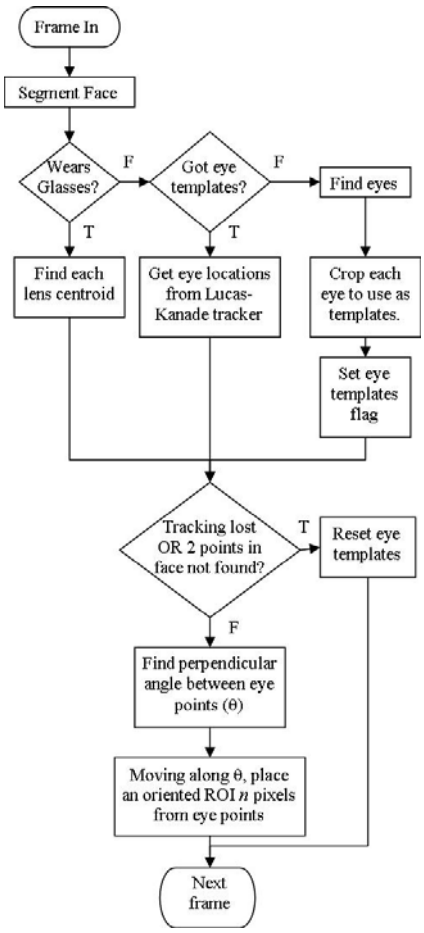

Figure 1 presents the major processes in the proposed blush detection framework. The 'segment face', 'wears glasses', 'find lens centroid', 'tracker' and 'find eyes' processes can be substituted for any alternative approach. However, an explanation of the algorithms employed in this implementation is provided forthwith.

### *2.1 Segment face*

Face segmentation is performed empirically and simply by employing Otsu's (1979) threshold algorithm, followed by three dilations and three erosions. Otsu's threshold selection method chooses the threshold to minimise the intra-class variance of the black and white pixels. In Otsu's method, the threshold is searched exhaustively to minimise the intra-class variance, defined as a weighted sum of variances of the two classes:

$$\sigma_w^2(t) = \omega_1(t)\sigma_1^2(t) + \omega_2(t)\sigma_2^2(t) \tag{1}$$

weights $w_i$ are the probabilities of the two classes separated by a threshold $t$ and $\sigma_i^2$ variances of these classes. Otsu shows that minimizing the intra-class variance is the same as maximising inter-class variance:

$$\sigma_b^2(t) = \sigma - \sigma_w^2(t) = \omega_1(t)w_2(t)\left[\mu_1(t) - \mu_2(t)\right]^2 \tag{2}$$

which is expressed in terms of class probabilities $w_i$ and class means $u_i$. The class probability $w_i(t)$ is computed from the histogram as,

$$\omega_1(t) = \sum_0^t p(i) \tag{3}$$

while the class means $u_1(t)$ is,

$$\mu_1(t) = \sum_0^t p(i) * x(i) \tag{4}$$

where $x(i)$ is the value at the centre of the $i^{\text{th}}$ histogram bin. Similarly, $w_2(t)$ and $u_i$ on the right-hand side of the histogram for bins greater than $t$. The class probability and class means can be computed iteratively. The algorithm based on Otsu's method is available in Matlab as a standard function and has been used in this study.

The binary morphological processes fill in small holes and reduce the width of the arms of the spectacles, sometimes the arms are removed completely. A connected components algorithm is then implemented and the largest component is retained while the others are neglected.

### *2.2 Segment glasses*

In the proposed implementation, the centroid of each lens is returned if the subject is wearing glasses. Therefore, this process amalgamates the 'wears glasses' and 'find centroids' functions.

The approach employed required filling in all holes in the segmented face. This is because glasses reflect the infrared emitted back, which causes glasses to be much darker than the rest of the face. This image was then xor'ed with the segmented face image, which creates another image where the background within the face is now the

foreground. Simply inverting the segmented face would not be suitable as the background surrounding the face is still present.

In order to detect the centroid of each lens, a search for the largest ellipse, which does not extend into the background of the image, is performed. The ellipse must conform to certain size, orientation and eccentricity constraints. The search may be performed iteratively (using ellipse fitting methodologies or elliptical Hough transform) or evolutionary by means of a genetic algorithm. Once the largest ellipse is found, perform the search again but restrict the search to the other regions of the image. If only one ellipse that conforms can be found, then the subject is wearing glasses but may not be facing the camera. If two ellipses conform then the user is wearing glasses and the centroids are used for ROI placement. The subject is judged to not be wearing spectacles if no ellipses that conform are found. If more than two ellipses are found then the frame is skipped.

An alternative, simpler, approach could be to erode the xor'ed image with a relatively large elliptical structural element (i.e., an ellipse that can fit within a lens but big enough to remove the nose). This should remove the mouth and nose, leaving blobs representing the internal of the lens. The centroid of which can be used as the centroid of the lens. However, the downfall of this approach is that it is not scale invariant.

It is also interesting to note that segmenting the glasses and finding the centroids of the lenses on every frame can be omitted. This is because the Lucas-Kanade tracker (Baker and Matthews, 2004) can track the initially detected centroids just as well.

### *2.3 Tracking*

In the proposed method, the eyes serve as reference points from which we can reliably position the ROI. It has been found that using feature-based eye detection methods do not migrate well between infrared images taken using different cameras. This is especially the case when images from a high-end, mid-wavelength infrared (MWIR) camera are compared with that of a low-end long-wavelength infrared (LWIR) camera, such as the Argus P7225 used in the trials. Therefore, the eye locations are initially detected when a subject blinks (further information is provided later).

Using the eye locations, templates centred on each point are obtained from the image and are used for tracking by the Lucas-Kanade tracker (Baker and Matthews, 2004). It was found that small templates were susceptible to blinking and would therefore move up and down with the blink. This in turn moves the ROI even though the face has not moved. By increasing the size of the template, it improved the robustness to blinking. A template with a width and height equal to the distance between the two eyes was implemented to ensure minimal movement during blinks.

### *2.4 Find eyes*

As aforementioned, the eyes are used as reference points for reliable positioning of the ROI in the proposed implementation. Initial testing employed a feature-based eye detection algorithm. However, the consistency of extraction reduced when switching between cameras and when the sample set was increased. This is why it was decided that the eye positions should be obtained from blinking as this was the only consistent characteristic across all videos.

Blinking is a spatio-temporal characteristic. The movement relating to blinking is localised in time and space (with respect to the head). This permits the blinking motion to be separated from head movement. The proposed algorithm employed a pre-existing blink detection algorithm (Gorodnichy, 2003), which determines the second order change in order to filter out the pixel changes attributed to head movement.

### *2.5 Tracking lost*

Tracking is a crucial part of the algorithm so it is vital to know when the tracking has been lost. When tracking is lost, the feature values are being extracted from the incorrect region causing inconsistencies in the data. Many things can cause the loss of tracking, such as fast movements that have a high frequency of direction changes or occlusion (essentially removing the feature from view, which is akin to turning away from the camera). This is a significant challenge when free head movement is permitted as the subject can do anything spontaneously.

A simple method for determining whether the tracking has been lost is to compute the Euclidean distance between the newly determined template and the previous template. If loss of tracking occurs, the templates will differ greatly as they will be from different regions of the image. A simple threshold can determine this. Failing which, some heuristic rules based on the old and new coordinates can be implemented. These rules could include a threshold on the distance between points in successive frames and the angle and distance between the two-eye positions.

### *2.6 ROI Placement*

If performed successfully, the algorithm at this stage should produce a set of coordinates for both eyes. The approach to placing the ROI is trivial. Firstly, the angle and the distance between both eyes are calculated using equations (5) and (6), respectively. The angle is rotated by $\pi$ / 2 to obtain its perpendicular, pointing down from the eyes [equation (7)].

$$\theta = \tan^{-1}\left(\frac{E_R^y - E_L^y}{E_R^x - E_L^x}\right) \tag{5}$$

$$D = \sqrt{\left(\left(E_R^y - E_L^y\right)^2 + \left(E_R^x - E_L^x\right)^2\right)} \tag{6}$$

where $E_R^x$ and $E_R^y$ are the *x* and *y* coordinates of the right eye, $E_L^x$ and $E_L^y$ are the *x* and *y* coordinates of the left eye.

$$\theta_p = \theta + \frac{\pi}{2} \tag{7}$$

From these equations, the centre of the ROI can be determined by simply moving along the perpendicular from each eye. These positions are determined using equation (8).

$$C_s^x = E_s^x + n\cos\theta_p, C_s^y = E_s^y + n\sin\theta_p \tag{8}$$

where $C_s^x$ and $C_s^y$ are the *x* and *y* coordinates of the ROI centre, *s* is used to denote whether left or right eye, *n* is the distance to the centre of the ROI from the eye (e.g., 0.75 * *D* / 2).

The ROI is an oriented, square window. This will provide robustness to roll rotation (tilt head either side) as this has been identified (empirically) as the most common rotation as most subjects tended to keep their eyes on the screen. The coordinates contained within the ROI are calculated using equations (9) and (10).

$$P_s^x = C_s^x + \left(d - \frac{sz}{2}\right)\cos\theta - \left(k - \frac{sz}{2}\right)\sin\theta \tag{9}$$

$$P_s^y = C_s^y + \left(d - \frac{sz}{2}\right)\sin\theta + \left(\frac{sz}{2} - k\right)\cos\theta \tag{10}$$

where *d* and *k* range from 0 to *sz*, *sz* is the dimension size of the window (e.g., 15 pixels), $P_s^x$ and $P_s^y$ are the *x* and *y* coordinates of a pixel location belonging to s ROI (*s* denotes left or right).

This algorithm provides a means to extract reproducible ROIs from images in both charge coupled device cameras (CCD) and thermal images from infrared cameras. Therefore, it can also be used to segment an ROI for determining change in coloration. A selection of screen dumps, as a result of the ROI segmentation algorithm, is provided in Figure 2.

**Figure 2** Example results of ROI segmentation algorithm

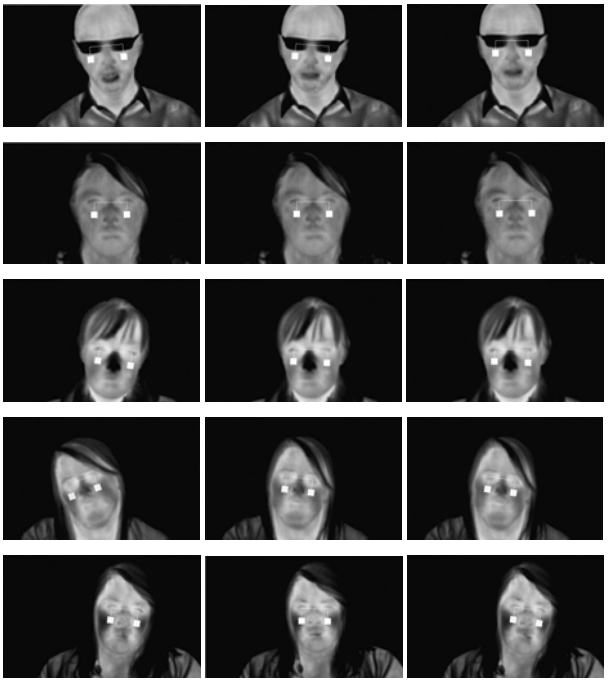

Note: Lines and squares shown for illustration purposes.

## 3 Proposed blush detection

Once the ROI has been segmented, feature values need to be extracted. In this implementation, the mean value [see equation (11)] from each ROI is used. The mean value was used because it is more robust to slight transformations of the ROI.

$$\mu_s(f) = \frac{1}{N} \sum_{x,y \in \left\{P_s^x,\, P_s^y\right\}} I(x, y) \tag{11}$$

where $I(x, y)$ is the greyscale value/temperature at the pixel located at $(x, y)$, $\{P_s^x, P_s^y\}$ are the set of coordinates belonging to $s$ ROI, $N$ is the total number of pixels in the ROI, $\mu_s(f)$ is the mean value of $s$ ROI ($s$ denotes left or right) for frame $f$.

The mean of both ROIs is determined for each frame of the video. As the base level temperature for each subject will vary, the proposed method employs an initial period from which baseline values can be determined. During the baseline period, the mean and standard deviations of each ROI for all frames within the baseline period is calculated [see equations (12) and (13)]. For all subsequent frames, the mean value obtained from each ROI is normalised using z-score normalisation [equation (14)].

$$\mu_b^s = \frac{1}{F_b} \sum_{f=1}^{F_b} \mu_s(f) \tag{12}$$

$$\sigma_b^s = \sqrt{\frac{1}{F_b} \sum_{f=1}^{F_b} \left(\mu_s(f) - \mu_b^s\right)^2} \tag{13}$$

$$z_s(f) = \frac{\mu_s(f) - \mu_b^s}{\sigma_b^s};\ \forall\left(f > F_b\right) \tag{14}$$

where $F_b$ is the number of frames in the baseline period.

It is assumed that the temperatures during the baseline period belong to one distribution and the temperatures during a blush response belong to another. Therefore, a simple threshold ($h$) based on the number of standard deviations from the baseline mean can be used. However, a blush response is not over instantaneously. In Kalra and Magnenat-Thalmann (1994), it is stated that blushing occurs within 2 seconds after presentation of the stimuli and can last up to 15 minutes, although the median was 20 seconds. It is not necessary to know when the blushing ceases, only to ensure that the temperature exceeds a level for a significant period. This condition is presented in equation (15).

$$blushing = \begin{cases} 1, & \text{if } (dT > \tau) \\ 0, & \text{otherwise} \end{cases} \tag{15}$$

where $dT$ is the time (continuous) above the standard deviation threshold ($z_s(f) > h$) for either the left or the right ROI, $\tau$ is the duration threshold.

## 4 Experimental results

For the experiments, the Argus P7225 from e2v was employed. This is a LWIR camera and operates near the plateau of the blackbody curve for temperatures around that of a human body. As it operates near the plateau, a small change in temperature will have less affect on the spectral radiance than that of a MWIR camera, which operates on a steep ascent. Therefore, MWIR cameras are better for measuring small changes where LWIR cameras are commonly used for firefighting activities. One reason for this is because the dynamic range automatically readjusts to the range of temperatures within the scene, which facilitates easy segmentation of extremely hot objects. LWIR cameras are also much cheaper than the MWIR cameras and it would be advantageous if the cheaper cameras can also detect changes in facial temperature.

### *4.1 Experimental setup*

As the Argus P7225 is a microbolometer-based camera, all temperatures within the field of view are used to determine the range. The camera then readjusts to the new range every so often. Therefore, in the experiments, it was paramount to ensure that no external heat sources can enter the field of view. This step is essential as the camera used only outputs image data and not temperature data. If the range changes too much, the greyscale values will not represent the same temperature as before. It is assumed that the greyscale values represent some unknown range of temperatures, which change when the range readjusts.

In order to test the proposed algorithm, the technique was implemented in conjunction with a psychophysiological experiment. The psychophysiological experiment attempted to determine the act of deceit by using visual stimuli to elicit a response. Prior to the experiment, individuals decided, in secret, whether they would try to deceive the system by concealing a banned object. In an attempt to elicit a response, the subject watched a video, which initially displayed calming images and audio (in order to obtain baseline values) prior to presenting images of many banned objects (the stressors), while the facial temperature was monitored throughout. Incentives and disincentives were also provided in an attempt to ensure the subjects made concerted efforts of deception and increased the emotional attachment to the object they were concealing.

It is hypothesised that subjects, who chose to conceal a banned object, will have an emotional attachment to an image of the object and potentially to the threat of the disincentive if they fail. At the point at which these stressors are presented, it is also hypothesised that the emotional response attributed to these stressors will manifest as an increase in facial temperature.

### *4.2 Results*

For the experiments, there were 53 subjects from which 27 did not try to conceal a banned object whereas 26 did. The subjects did not reveal whether they had attempted to deceive the system until after the experiment. The analysis was performed offline, although it can be adapted to be performed during the test.

The analysis consisted of a multitude of permutations of the adjustable parameters. These parameters included the number of standard deviations ($h$ – from 0.5 to 10 standard deviations) for the temperature threshold, the threshold for the duration

above the temperature threshold ($\tau$ – 0.5 s to 3 s) and the duration of the period from which the baseline (*blp* – 5 s to 19 s) data was extracted. The threshold, *h*, is based on the assumption that blushing and baseline temperatures belong to separate distributions and provides a contextual element to the calculation. This is because the subject's internal temperatures and blush responses are unique. In the event that the assumption seems wrong, additional tests were conducted whereby the values obtained during stimuli presentation were not *z*-score normalised but simply mean adjusted to the baseline mean. An incrementing threshold on the positive deviation from the mean was used to determine blushing.

**Figure 3** ROC curve – *z*-score threshold (see online version for colours)

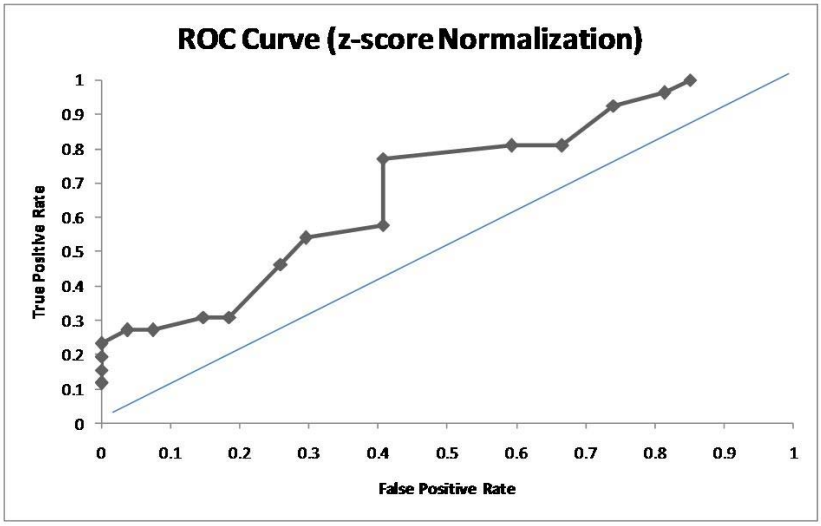


**Figure 4** ROC curve – mean adjusted threshold (see online version for colours)

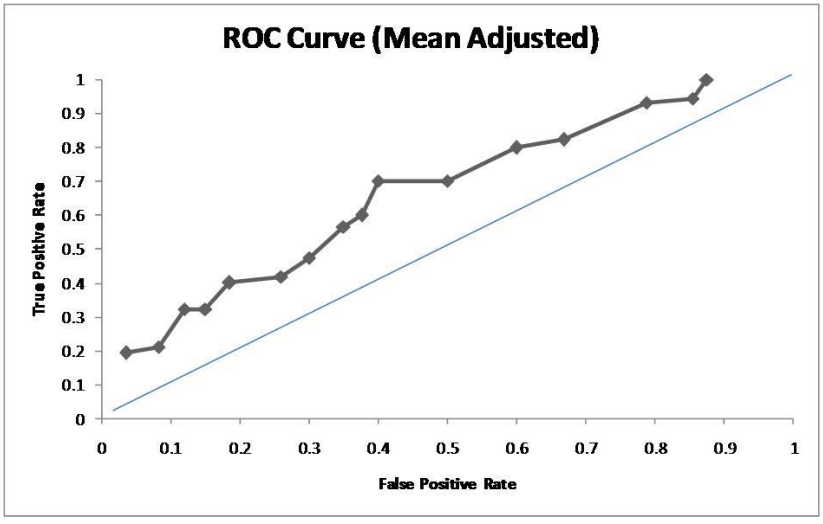

As the number of trials is too large to present in its entirety, the optimal receiver operating characteristic (ROC) curve, for both the *z*-score and mean adjusted threshold, is presented in Figures 3 and 4. Figure 3 is the ROC curve obtained when 15 seconds of baseline values were used and a continuous duration above the threshold of 2 seconds. Whereas, Figure 4 was the result of extracting 10 seconds of values to be used as baseline and a continuous duration above the threshold of 2.5 seconds.

It is immediately obvious from both ROC curves that the results lay on the preferred side of the linear function $x = y$ (as depicted on the graphs). This indicates that the classifier provides better classification than random selection. The optimum threshold from Figure 3 was three standard deviations, which resulted in ~77% true positive rate (TPR) and ~60% true negative rate (TNR). This gives an accuracy of the classifier as ~67%. This is slightly better than the optimal results from Figure 4 (~65% accuracy).

The accuracy is encouraging as it is better than expected. Previous trials with the P7225 thermal camera indicated that blushing can be detected, although this was when blushing was elicited through embarrassment. This resulted in a strong response. However, it is not known how strong the response will be from using visual stimuli and whether it would be detectable. Coupling this uncertainty with a low-end infrared camera, which is not designed for detecting small temperature changes, the original expectation was that the accuracy would be nearer 50% (i.e., not much better than random classification). As the optimal accuracy was 67%, the results are encouraging. However, additional enhancements can possibly improve the accuracy.

### *4.3 Discussion*

In the experiments, a low-end long wave infrared (LWIR) thermal camera was implemented. As mentioned this is not the ideal camera for this application and the algorithm would benefit from a high-end medium wave infrared (MWIR) camera, although these currently are very expensive. A MWIR thermal camera will provide greater resolution, which will not only improve the accuracy of the readings, but also permit improved tracking and landmark localisation as the local structure will be better defined. Although the system will benefit from employing a more suitable infrared camera, the main contributor to anomalies is movement.

Movement of the subject is the primary cause of reduced overlapping between ROI of different video frames. The ROI should overlap 100% to ensure the same relative region of the face is captured. However, ensuring optimal overlapping is a non-trivial task when there are no constraints placed on the user. During the trials, it seemed that the algorithm proposed was robust to translations and for roll rotations, which seemed more frequent in the trials, but was susceptible to yaw (‘no’ head movement) and pitch (‘yes’ head movement) rotations.

An approach to improve robustness to these rotations could be to use the Lucas-Kanade tracker to estimate the warping of the image and apply to the shape of the ROI. Alternatively, the thermal image can be fused with an image from a video camera. Then active appearance models (AAM) (Cooteset al., 2001) can be used to model the warping of the face under movement and the ROI can simply be the triangle, in the triangulated mesh, that represents the upper cheek. The AAM approach would be more suitable than the Lucas-Kanade method as it uses landmarks to position the mesh and the ROI shape will have greater flexibility. However, it is more computationally complex and

it may not result in significant improvement with large rotations. This is because the vast majority of the ROI may not actually reside within the scene any longer. The only single-camera solution to capture the ROI under all rotations is to move the camera so the subject is always directly facing the camera. Alternatively, additional cameras can be employed at further expense. It should also be noted that this problem is being investigated in Zhou and Tsiamyrtzis (2008, 2009) where they are attempting to track facial tissue under varying orientations.

On the other hand, visual elicited blush response often shows other detectable temperature cues in other regions of the face, side of the neck and measurable heart beat changes as well (Harmer et al., 2010). The presented method, which is developed empirically, has achieved a good detection rate; however, it is still far from the standard of actual applications. Systematic methods should be employed and compared to further investigate these critical cues in order to improve the overall detection rates to practical level.

## 5 Conclusions

An approach to automatic blush detection has been proposed in this paper. This algorithm has been applied to a psychophysiological experiment which investigated whether visual cues can elicit a blush response that will betray a subject's intention. The underlying framework of the algorithm permits interchangeable modules which increases the flexibility. In its current form, the algorithm is robust to migration between different thermal cameras and CCD cameras as the act of blinking is detectable in all images (with the exception of bespectacled subjects). Therefore, the ROI segmentation method can be used to detect coloration or thermal activity within a consistent local area.

From the experiments conducted, a classification accuracy of ~67% was achieved. This is somewhat encouraging as a low end thermal camera was implemented. Although, some of the errors are attributable to the type of camera employed, movement is still the main contributor to errors. The algorithm proposed seemed robust for roll rotations, which seemed more frequent in the trials, but was susceptible to yaw ('no' head movement) and pitch ('yes' head movement) rotations. This is due to the reduced overlapping between ROIs while the head undergoes these rotations.

An approach to improve robustness could be to use the Lucas-Kanade tracker to estimate the warping of the image and apply to the shape of the ROI. Alternatively, the thermal image can be fused with an image from a CCD camera. Then AAM (Cootes et al., 2001) can be used to model the warping of the face under movement and the ROI can simply be the triangle, in the triangulated mesh, that represents the upper cheek.

## Acknowledgements

The authors thank the project sponsor, colleagues, and partners in the e2v Technology for their kind supports.

## References

Baker, S. and Matthews, L. (2004) 'Lucas-Kanade 20 years on: a unifying framework', *International Journal of Computer Vision*, Vol. 56, No. 3, pp.221–255.

Cootes, T.F. et al. (2001) 'Active appearance models', *IEEE Transactions on Pattern Analysis and Machine Intelligence*, Vol. 23, pp.681–685.

DeJong, P.J. et al. (2002) 'Blushing after a moral transgression in a prisoner's dilemma game: appeasing or revealing?', *European Journal of Social Psychology*, Vol. 32, pp.627–644.

Drummond, P.D. and Lim, H.K. (2000) 'The significance of blushing for fair- and dark-skinned people', *Personality and Individuality Differences*, Vol. 29, pp.1123–1132.

Fukuda, K. (2001) 'Eye blinks: new indices for the detection of deception', *International Journal of Psychophysiology*, Vol. 40, No. 3, pp.239–245.

Gamer, M. et al. (2006) 'Psychophysiological and vocal measures in the detection of guilty knowledge', *International Journal of Psychophysiology*, Vol. 60, No. 1, pp.76–87.

Gorodnichy, D. (2003) 'Second order change direction and its application to blink-controlled perceptual interfaces', *Proceedings of IASTED Conference on Visualization, Imaging and Image Processing*, Benalmadena, Spain.

Gronau, N. et al. (2005) 'Behavioural and physiological measures in the detection of concealed information', *Journal of Applied Psychology*, Vol. 90, No. 1, pp.147–158.

Harmer, K., Yue, S., Guo, K., Adams, K. and Hunter, A. (2010) DiPP Technical Report II on Algorithms, October.

Kalra, P. and Magnenat-Thalmann, N. (1994) 'Modelling of vascular expressions in facial animation', *Proceedings of Computer Animation*.

Mulkens, S. et al. (1997) 'High blushing propensity: fearful preoccupation or facial coloration', *Personality and Individuality Differences*, Vol. 22, No. 3, pp.817–824.

Mulkens, S. et al. (1999) 'Fear of blushing: fearful preoccupation irrespective of facial coloration', *Behaviour Research and Therapy*, Vol. 37, pp.1119–1128.

Otsu, N. (1979) 'A threshold selection method from gray-level histograms', *IEEE Transactions on Systems, Man, and Cybernetics*, Vol. 9, No. 1, pp.62–66.

Pavlidis, I. et al. (2002) 'Seeing through the face of deception', *Nature*, Vol. 415, pp.35–36.

Pollina, D.A. et al. (2006) 'Facial skin surface temperature changes during a 'concealed information' test', *Annals of Biomedical Engineering*, Vol. 34, No. 7, pp.1182–1189.

Shastri, D. et al. (2008) 'Periorbital thermal signature signal extraction and applications', Presented at the *IEEE Conference on Engineering in Medicine and Biology Society*.

Shearn, D. et al. (1990) 'Facial colouration and temperature responses in blushing', *Psychophysiology*, Vol. 27, No. 6, pp.687–693.

Tsiamyrtzis, P. et al. (2005) 'Imaging facial physiology for the detection of deceit', *International Journal of Computer Vision*, Vol. 71, No. 2, pp.197–214.

Vershuere, B. et al. (2004) 'Autonomic and behavioural responding to concealed information: differentiating orienting and defensive responses', *Psychophysiology*, Vol. 41, No. 3, pp.461–466.

Zhou, Y. and Tsiamyrtzis, P. (2008) 'A probabilistic template update method for tracking facial tissue in thermal infrared', *Proceedings of 5th International Conference on Advanced Video and Signal Surveillance.*

Zhou, Y. and Tsiamyrtzis, P. (2009) 'Tissue tracking in thermo-physiological imagery through spatio-temporal smoothing', *Proceedings of 12th International Conference on Medical Image Computing and Computer Assisted Intervention (MICCAI 2009)*, pp.1092–1099.

Zhu, Z. et al. (2007) 'Forehead thermal signature extraction in lie detection', *Proceedings of 29th International Conference of the IEEE Engineering in Medicine and Biology Society*, pp.243–246.

Zhu, Z. et al. (2008) 'The segmentation of the supraorbital vessels in thermal imagery', *IEEE Conference on Advanced Video and Signal Based Surveillance*, pp.237–244.